Mechanical Constraint and Release Generates Long, Ordered Horizontal Pores in Anodic Alumina Templates

Ciara T. Bolger [†,‡], *Giovanni Fois*[‡], *Nikolay Petkov*[†,‡], *Nicolas Sassiat*[⊥], *Micheál Burke*[⊥], *Aidan J. Quinn*[⊥], *Graham L. W. Cross*[§,‡*], *and Justin D. Holmes*[‡,†*]

[†]Materials Chemistry and Analysis Group, Department of Chemistry and the Tyndall National Institute, University College Cork, Cork, Ireland.

[‡]Centre for Research on Adaptive Nanostructures and Nanodevices (CRANN), Trinity College Dublin, Dublin 2, Ireland.

[⊥]Nanotechnology Group, Tyndall National Institute, University College Cork, Lee Maltings, Dyke Parade, Cork, Ireland.

[§]School of Physics, Trinity College, Dublin 2, Ireland.

*To whom correspondence should be addressed. E-mail: CROSSG@tcd.ie or j.holmes@ucc.ie; Tel: +353 (0)21 4903608, Fax: +353 (0)21 4274097

Abstract

We describe the formation of long, highly ordered arrays of planar oriented anodic aluminium oxide (AAO) pores during plane parallel anodisation of thin aluminium "finger" microstructures fabricated on thermally oxidised silicon substrates and capped with a silicon oxide layer. The pore morphology was found to be strongly influenced by mechanical constraint imposed by the oxide layers surrounding the Al fingers. Tractions induced by the SiO_2 substrate and capping layer led to frustrated volume expansion and restricted oxide flow along the interface, with extrusion of oxide into the primary pore volume, leading to the formation of dendritic pore structures and meandering pore growth. However, partial relief of the constraint by a delaminating interfacial fracture, with its tip closely following the anodisation front, led to pore growth that was highly ordered with regular, hexagonally packed arrays of straight horizontal pores up to 3 µm long. Detailed characterisation of both straight and dendritic planar pores over a range of formation conditions using advanced microscopy techniques is reported, including volume reconstruction, enabling high quality 3D visualisation of pore formation.

KEYWORDS. AAO, mechanical constraint, anodisation, stress, pores, planar, order

1. Introduction

Anodic aluminium oxide (AAO) is a common host material to template the growth of ordered arrays of semiconducting[1-5] and metallic[6-9] nanowires and nanotubes[10,11] by various methods, including chemical vapor deposition (CVD)[2,4], supercritical fluid (SCF) deposition[1,3], electrochemical deposition[6-9] and self-assembling methods.[10] These self-organised templates demonstrate potential for enabling the integration of ordered nanostructured arrays into functional electronic devices.[12-14] Such devices could require Al to be anodised in a planar orientation, within multilayered device architectures, such that the encapsulated nanostructures, under strict dimensional control and precision placement, could be exploited, *e.g.* as high density metal interconnects. Importantly, nanostructure arrays produced by plane parallel AAO could potentially be integrated with planar integrated circuits, which is not the case for the commonly used vertical template.

Masuda and co-workers[15] were the first to report the generation of a two dimensional porous AAO template with pores parallel to the substrate, produced through the anodisation of an aluminium film deposited on a glass slide and covered by a sputtered aluminium oxide layer. The edge of the sandwiched Al was exposed to the electrochemical bath and a horizontal porous structure was achieved. Recently, other groups have realised similar horizontally-oriented nanochannels following this idea.[16-19] In these reports, an aluminium film deposited onto an oxidised silicon substrate was etched in parallel strips and then capped with a silicon oxide layer.[16-19] The short edges of the strips were dipped into the electrolyte and the anodisation proceeded along their lengths. Cojocaru and co-workers[17] have shown scanning electron microscopy (SEM) and transmission electron microscopy (TEM) images of horizontal pores, 200-300 nm long, with pore diameters

between 3-4 nm. Xiang and co-workers[16] reported the fabrication of horizontal porous templates with controlled pore diameters between 10-130 nm and interpore distances ranging from 30-275 nm, and described a transition from a hexagonal to a square arrangement in the pore ordering when the interpore distance increased to about one quarter of the 225 nm film thickness. Gowtham *et al.*[18] reported the fabrication of arrays of in-plane nanopores within patterned Al fingers wedged between SiO_2 layers with a mean pore diameter of 20 nm. Recently, Xiang *et al.*[19] demonstrated the concept of multi-contact anodisation on a single chip, in which Al fingers were individually anodised with either sulfuric, oxalic or phosphoric acid at different applied voltages ranging between 20-110 V. On a single chip, two Al fingers were contacted and anodised separately, one at 50 V with phosphoric acid, and the other at 40 V with oxalic acid to obtain mean pore diameters of 80 and 27 nm respectively.

As with all porous systems, complete morphological characterisation requires determination of pore length and direction/orientation, morphology and ordering of pores, as a function of length. With the exception of Cojacoru *et al.*, the work cited above reports structural characterisation of the confined planar AAO through analysis of pore nucleation and arrangement of pores at the surface only, with no measurement of ordering as a function of length along the pore array. For example, Masuda *et al.* estimated the pore length from the anodisation time.[15] Estimation of pore length from the anodisation time assumes the formation of straight pores oriented perpendicularly to the imaged surface at the same rate as vertical AAO formed in an Al foil. However, currently there is no direct evidence to support this assumption. Gowtham *et al.* include an image of a 'front on' section exposed by a focused ion beam along the anodised Al finger length.[18] The distance of this section from the edge was not defined, and since the image shown was not related to any image at the

surface, no 3D information was provided from this section. Xiang *et al.* included a growth rate but no physical characterisation of pore length, morphology or ordering as a function of length.[19] An exhaustive study regarding in plane pore growth of confined Al fingers, including pore length and direction/orientation, morphology and ordering of pores, as a function of length, is therefore still required. Such a characterisation study will provide insight into the fundamental processes governing AAO pore formation in a constrained environment and enable subsequent exploitation of the governing factors to prepare highly ordered, long, planar oriented AAO, which has not yet been reported.

The influence of mechanical stress on pore formation within vertical AAO membranes was first reported by Jessensky *et al.*[20], who suggested that stress is induced at the metal/oxide interface during the anodisation process due to the volume expansion associated with aluminium conversion to aluminium oxide. The induced interfacial stress is believed to be the origin of pore self-organisation in free-standing vertical AAO membranes producing hexagonally ordered porous templates. Later, Garcia-Vergara *et al.*[21] employed a tungsten tracer to show that vertical AAO pores form in Al foils anodised in phosphoric acid due to the flow of Al_2O_3 in the barrier layer region beneath the porous layer. During the anodisation process, aluminium oxide migrates through the barrier layer region toward the metal interface, then outward and upward in the oxide pore walls. This path of oxide movement was suggested to be facilitated by the field-assisted plasticity of the oxide film material and driven by growth stresses within the film. Recently, Houser *et al.*[22], using finite element analysis, simulated the viscous flow of oxide as generated by local compressive stresses close to the pore base under steady state anodisation conditions, in a geometric domain based on one cell of porous anodic alumina. This compressive interfacial stress may result from the competition between anion adsorption and oxide growth at these sites.

The effect of externally induced stress on Al anodisation has been studied by Sulka and co-workers.[23] ~~Al anodisation was carried out under an externally applied tensile stress, by clamping the Al foil into a holder in contact with a ceramic plate which was then screwed from the opposite side to apply a 'low' or 'high' tensile stress, depending on the number of rotations of the driving screw. The Delaunay triangulation method was used to determine the number of defects present within the AAO film.~~ The number of defects observed in the AAO membrane was directly related to the degree of external stress during anodisation for levels ranging as 'non-stressed', 'low stressed' and 'highly stressed'. The vertical anodisation of mechanically constrained aluminium is known to induce compressive stress at the aluminium/confining wall interface.[24] The retardation of the anodisation rate has been observed in the vertical anodisation of aluminium within patterned trenches, as a result of the contact between aluminium and the vertical sidewalls, which inhibits the linear vertical expansion of the AAO developing at this interface. The boundary between the AAO which develops and the remaining aluminium forms a curved interface due to this retarded AAO growth rate at the Al/trench sidewall interface, compared to the rate of AAO formed in the centre of the confining trench.[24] A similar curved AAO/Al interface was observed when a patterned substrate with alternating regions of aluminium and thick barrier layers of aluminium oxide was anodised on a SiO_2-coated Si wafer at 40 V with oxalic acid.[25] ~~The dense aluminium oxide barrier layer used to pattern the substrate remained firmly attached to the aluminium during anodisation and prevented pore formation in the underlying aluminium in these regions.~~ The profile of the AAO formed in the aluminium/aluminium oxide boundary regions was shown to be curved with retarded pore growth close to the barrier oxide film.[25] In the case of highly confined structures, such as encapsulated aluminium films for horizontal pore templates, mechanical stress induced by both volume expansion and oxide flow greatly affects pore development and morphology. Very recently, Oh *et al.*[26]

showed cross sectional SEM micrographs of dendritic structures formed when anodising an aluminium film sandwiched between silicon oxide layers. They suggested that dendritic porous templates form due to the restriction of aluminium oxide flow by traction at the Al/silicon oxide interface.

In this paper we analyse pore development in a mechanically constrained template, where a patterned aluminium film is sandwiched between two silicon oxide layers. For the first time, an ordered array of horizontal AAO pores ~ 3 μm long is shown by cross sectional TEM along the pore axes. There have been few reports of horizontal oriented AAO pores. None have explicitly demonstrated straight, ordered, horizontal AAO pores that extend for distances of several micrometers. The influence of film constraint on the pore morphology is discussed in light of these results. In particular, the relationship between porous dendritic structures and the stress developed during the anodisation process is considered.

2. Experimental Methods

Substrate Fabrication and Preparation. Substrates consisted of p-type Si wafers terminated by a thermally grown 500 nm silicon dioxide (SiO_2) layer with a 5 nm Al_2O_3 adhesion layer. Al (99.999 %) films for anodisation, either 200 or 550 nm thick, were deposited on these substrates by electron-beam evaporation using a *Temescal FC-2000.* The Al film was then patterned into fingers 40 μm long and 2, 4 or 6 μm wide, in the centre of each 1 cm^2 chip of 10 cm wafers by metal lift off from the underlying optical lithography mask. These fingers were connected to a square Al contact pad on the corner of each chip. Fingers of Al 200 nm thick were then sputter coated with SiO_2 to a nominal thickness of 300 nm (substrate type I)

and fingers of Al 550 nm thick were sputter coated with SiO_2 to a thickness of 800 nm. The SiO_2 layer was also patterned by lift off. Anisotropic wet etching of Al, using a solution of H_3PO_4/HNO_3/acetic acids, was then used to expose the Al finger edge. In the case of the 550 nm thick Al fingers, controlled over-etching of the Al fingers enabled variation of the SiO_2 layer thickness from 250 to 800 nm over the first ~ 5 μm of the finger length (substrate type II). Figure 1 displays TEM cross sections of the two substrates used, type I: Al 200 nm thick and SiO_2 300 nm thick, and type II: Al 550 nm thick and SiO_2 thickness varied between 250 and 800 nm. Following dicing of the wafer into 1 cm^2 chips, focused ion beam (FIB) milling was used to polish the end of each Al finger; using a 30 kV accelerating voltage in two steps, *i.e.* at 1 nA and 93 pA, to ensure a flat edge perpendicular to the Al finger length, so that the anodising current was directed parallel to the Al surface.

Anodisation of Substrates. Anodisation was carried out in a custom built electrochemical cell with the chip held at a constant separation of 6 cm from the lead counter electrode. Electrical contact to the Al fingers was improved by applying silver contact paste (*Agar Scientific*) to the exposed Al pad. The chip was then partially immersed in the electrochemical bath and anodised at a constant potential using a direct current (dc) power supply (*Thurlby Thandar Instruments model EX752M*). Three different electrolytes were prepared for the electrochemical process: 2 M sulfuric acid (H_2SO_4), 0.3 M oxalic acid ($H_2C_2O_4$) and 1 M phosphoric acid (H_3PO_4). Different voltages, temperatures, anodisation times were employed: substrates were potentiostatically anodised over a range of 10-130 V at room temperature or cooled down to 0-5 °C for between 30 min and 8 h. Each anodisation was carried out using the electrolyte for which the voltage applied was within a self ordering regime.

Characterisation. Samples were imaged by scanning electron microscopy (SEM) and prepared for analysis by transmission electron microscopy (TEM) on a *FEI Helios NanoLab 600i* dual-beam focused ion beam (FIB) instrument. SEM images were acquired at 5 kV & 47 pA as standard using the through lens detector (TLD) in high resolution mode. Gold and palladium were sputtered onto the surface of some samples before SEM imaging to reduce charging effects (Agar sputter coater operating at ~37 mA). The resulting porous fingers were analysed by serial sectioning via FIB milling and SEM imaged with the *Helios NanoLab 600i* system. No metal rich layer was deposited due to the presence of a SiO_2 directly above the porous layer which served as a protective coating. A 30 keV ion beam at a current of 1 nA was used to expose the region of interest with a cross sectional mill. Subsequently, serial milling was carried out at the lowest possible beam current of 9.3 pA over a total length of ~4 μm. SEM micrographs acquired during the sectioning procedure were used to reconstruct the volume of individual pores within the anodised samples. For TEM cross section specimen preparation a platinum rich protective layer was built up over the site of interest using electron beam induced, and ion beam induced deposition steps with a Pt gas injection system on the FIB. A lamella was then isolated with FIB milling and undercut at 45˚ to the ion beam. Once attached to the micromanipulator probe (*Omniprobe* Micromanipulator) with Pt, the lamella was cut free from the substrate and reattached to a TEM half grid. TEM images were acquired with a *JEOL 2100* high-resolution instrument operating at 200 kV.

Volume Reconstruction. Volume reconstruction was carried out using the 3D visualisation software *Amira*, from Visage Imaging. The reconstruction process incorporated the following steps: (a) correction of voxel (3D pixel) dimensions for oblique-angle imaging (52 degrees), (b) digital image alignment to compensate for *x–y* drift (image registration).

Although an effort can be made to obtain well aligned images during the sectioning process, these images are always offset to some extent due to thermal drift of the stage and mechanical system instabilities. In particular, for a given sequence of images, an intrinsic shift of the included features was observed in the y direction since the images were acquired at a tilt of 52˚ to the electron beam. Therefore, alignment of the stack was carried out in pairs of consecutive sections until sub-10 nm resolution, or a so called 'quality function' of close to 100 %, was achieved; (c) crop-out of a suitable sub-volume; (d) image segmentation into material categories. The segmentation of images can be carried out using an automatic function based on pixel brightness levels, or manually by selection of pixels deemed to belong to a particular material category, in this case simply 'pore' or 'oxide' and (f) 3D visualisation and representation. False colouring was applied to the image segments, to highlight the different parts of the reconstructed volume.

3. Results and Discussion

Horizontal anodisation of aluminium thin films was carried out for aluminium fingers sandwiched between insulating SiO_2 films. This configuration ensured that the electric field was directed parallel to the surface of the evaporated Al film. Figure 1 depicts a schematic of the substrates and characterisation steps used for the planar anodisation process. Figures 1 (b) and (c) present TEM cross sections along the length of an as-fabricated Al finger from each of the two substrate types, before anodisation. As mentioned above, the stress induced by anodisation in this mechanically constrained environment strongly affects the morphology of the resultant AAO pores. Figures 1 (d) and (e) depict the resultant AAO obtained for the two substrate types. For samples with a 200 nm thick Al film and uniform, 300 nm thick

SiO_2 capping layer (substrate type I), the capping layer always remained intact throughout the anodisation process. We infer that a high level of stress was generated within the aluminium film, leading to the observed dendritic pore growth similar to results shown by Oh *et al*.[26] Alternatively, for samples with a 550 nm Al film and non-uniform SiO_2 capping layer that ramped from 250 to 800 nm thickness along the axis of the finger (substrate type II), the SiO_2 capping layer was partially removed due to delamination from the alumina film. Stress induced by aluminium oxide formation was relieved in the delaminated region yielding straight pores while the closed region with the intact SiO_2 capping layer showed dendritic pore formation.

Substrate Type I. Anodisation of 200 nm thick Al fingers deposited on thermally oxidised silicon substrates (500 nm oxide thickness) and coated with a 300 nm SiO_2 capping layer resulted in the formation of AAO films with visible 'front-on' pore openings. Figure 2 shows typical SEM images for type-I substrates anodised under various conditions: (a) with H_2SO_4 at an applied voltage of 20 V, (b) with $H_2C_2O_4$ at 40 V, (c) with H_2SO_4 at 80 V and (d) with $H_2C_2O_4$ at 130 V. An empirical relationship between the mean pore diameter (D_P) and the applied voltage (V) was determined by analysing the SEM micrographs. Values for D_P were obtained from Lorentzian pore diameter distributions for anodisations over the applied voltage range between 10-130 V, as detailed in Supplementary Information, Figure S1. O'Sullivan and Wood first showed that D_P is directly dependent on the applied voltage according to the equation $D_P = k_p V$.[27] The linear coefficient k_p for vertical pores grown on thick aluminium foils was found to be 1.29 nm V^{-1}. A plot of pore diameter vs. voltage for our data is shown in Figure 3. From a linear fit we find the coefficient k_p to be 0.26 nm V^{-1}, a marked decrease from the reported value for Al foils. A decrease in k_p to 0.9 nm V^{-1} has previously been reported for vertically anodised Al films supported on Si substrates.[28]

This apparent decrease in k_p was rationalised as a voltage drop across the semiconducting Si wafer thickness, as contact was made to the Al from the back of the doped Si wafer. However, recently we reported the case of vertical anodisation of supported Al thin films on silicon where contact was made directly to the Al. In this case, a significant drop in the value of k_p to 0.5 nm V^{-1} was still observed.[29] Thus, we find the drop to be a real phenomenon. We attribute the effect to the silicon substrate which may induce residual stress in the initial evaporated Al film, limiting plastic flow and inhibiting expansion of the alumina film in the lateral directions. This effect has also been reported by other researchers.[30] The presence of four Al/SiO_2 interfaces in this study should result in even greater mechanical constraint: a further reduction in k_p is therefore not surprising. In addition, we anticipate an electrostrictive stress at the anodisation front due to the establishment of a charge capacitor consisting of electrolyte/SiO_2/Al layers in unanodised regions. However, for the voltages used, we calculate this electrostriction to be a minor effect on the order of a few MPa, much smaller than the > 100 MPa stress that might be expected from frustration of volume expansion and plastic flow. The images displayed in Figure 2 are selected examples from the range of conditions used. These images are comparable to those published by Xiang *et al*., Gowtham *et al*., Zhang *et al*., and Kim *et al*.[18,19,31,32] In all cases the pores appear to be oriented horizontally but it is difficult to detect any hexagonal ordering.

Pore development along the anodisation direction, which is critical to our study, was investigated by the preparation of longitudinal cross sectional specimens. Subsequent TEM analysis revealed pores less than 2 μm long, despite the relatively long anodisation times used. In addition to the disordered pore arrangement observed from the 'front on' SEM images presented in Figure 2, a number of defects can be identified along the pore length. These include pore meandering, dendritic 'fish-boning' and dendritic pore splitting. Figure 4

displays some examples of porous structures obtained at different anodisation conditions. Figure 4 (a) shows a 200 nm film anodised with oxalic acid at an applied voltage of 40 V for 7 h, while the insets (b) and (c) display magnified views of the branched pore ends and pore openings from Figure 4 (a), respectively. Dendritic pore splitting of the two primary pores is observed, along with dendritic 'fish-boning' of both the primary and secondary pores. The front view of this substrate can be seen in Figure 2 (b). The length of the nanochannels for these anodisation conditions was ~1.5 μm. Figure 4 (d) displays a cross sectional view of a sample anodised with sulfuric acid solution at 10 V for 3 h. The pores extend for ~500 nm and a highly defective structure also develops under these conditions. Finally, a cross section of the substrate shown in Figure 2 (d) is presented in Figure 4 (e). The substrate was anodised in oxalic acid at 130 V for 3 h producing ~300 nm long pores with many secondary branches from the single primary pore stem.

Our results show that specific application of mechanical constraint of the anodising Al finger can control pore morphology, resulting in anything from highly ordered arrays through heavily defective dendritic forms. It is believed that the plastic flow of alumina is prevented along bounding interfaces due to adhesive tractions. As discussed by Oh *et al.*,[26] the pore formation by plastic flow in the expected horizontal pore growth direction is inhibited by traction at the pinned SiO_2 interfaces, so the extra volume of newly formed Al_2O_3 extrudes inside the primary pore, leading to the dendritic 'fish-boned' structure. The formation of such oxide 'fins' along the oxide/SiO_2 interface disrupts the stress gradients within the AAO film, which determine the direction in which the aluminium oxide flows. This may result in a 'knock on' effect of oxide flow into neighboring pores, and the development of 'fish-bone' structured pores throughout the Al finger thickness. The pore meandering and dendiritc splitting is likely to be a consequence of a rough Al/SiO_2 interface, as can be seen in Figures

4 (a) and (b). Such pore bending and branching have been observed in studies on the anodisation of curved surfaces by Lelonek *et al.*[33]

Given that the expansion associated with AAO formation is related to the anodisation voltage,[34] Oh *et al.* proposed that anodisation at low applied voltage, when the expansion coefficient (volume of porous AAO formed/volume of Al consumed) is close to unity, should minimise the effects of confinement on horizontal AAO formation, and result in straight rather than dendritic structures. However, in our study, even at an applied voltage of 10 V, we observed branching of the pore structure, as shown in Figure 4 (d). We conclude that the formation of oxide 'fins' will occur under any conditions of mechanically constrained formation, regardless of the expansion coefficient, resulting in an overall dendritic pore morphology. This morphology occurs because oxide flow along the SiO_2 interfaces is a requirement for horizontal pore formation.

Substrate Type II. Anodisation experiments were also performed using substrates containing a thicker Al film of 550 nm with a graded SiO_2 capping layer where the thickness was varied from 250 to 800 nm. A remarkable difference was observed in these samples compared to type I substrates. In the first 4.5 microns the SiO_2 capping layer thickness gradually increased from approximately 250 to 800 nm on the surface of the 550 nm Al film (see Figure 1), such that the component of top-side constraining force acting at the travelling anodisation front increases throughout this region. Transverse cross section SEM images of the resultant samples, displayed in Figure 5, showed partial delamination of the Al film from the underlying SiO_2 and in most cases delamination of the capping SiO_2 film. Where the capping silica was significantly thinner than the Al, delamination was observed. Thinning of the SiO_2 layer reduced its stiffness, such that the constraining stress was weaker at the

SiO_2/AlO_x interface leading to delamination in this region. Figures 5 (a) to (d) display identical Al fingers (all 4 μm wide) anodised at increasing voltages, from 20 to 80 V, at 20 V increments. From these images we observed that as the applied voltage was increased, the degree of delamination from the substrate also increased, when other conditions of anodisation (electrolyte, temperature, anodisation time *etc*.) were held constant. Given that the anodisation voltage affects the rate of anodisation through higher current density, this can be understood to determine the extent of delamination. We repeated anodisation at 80 V with H_2SO_4 for 30 minutes and 5 hours. These samples anodised at the same voltage but for different times showed little difference in the extent of the delamination. This provides strong evidence that the anodisation voltage alone determines the extent of delamination. The magnitude and even physical mechanisms of stresses induced by anodisation are already known to be highly dependent on the oxide formation rate[35] which supports the theory that stress induced during the anodisation process initiates substrate delamination. This delamination is only possible when the capping silica is below a threshold thickness.

A finger of one such sample that had been anodised at 80 V with H_2SO_4 was subsequently cross sectioned with a focused ion beam to expose different transverse sections of this SiO_2 'cap-free' region (see Figures 5 (e) to (g)). After anodisation, the tips of the pores in this delaminated region resemble alumina nanotubes (Figure 5 (f), inset), however, upon exposing a section along this region, highly ordered, hexagonally arranged pores were visible, which were significantly different to the disordered pores obtained with the 200 nm thick films (see Figures 5 (e) and (g)). We believe that the overall increased expansion, and increased stress associated with anodisation of such a film, along with the reduction of the SiO_2 thickness such that the imposed constrictive force is reduced results in partial delamination of the alumina film and also of the SiO_2 capping layer. During this process the stress associated

with the mechanical constraint at the anodisation front is relieved and straight, horizontal pores result.

FIB sectioning was carried out for ~ 4 μm in total along one such sample. Serial sectioning for part of this region yielded a stack of micrographs which imaged a length of over 2 μm at 30 nm intervals. Using *Amira* software these images were used to reconstruct the sectioned volume. Figure 6 displays two reconstructed sub-volumes obtained from stacks of images acquired along the pore length. Figure 6 (d) illustrates a straight horizontal pore which was reconstructed from images sectioned in the SiO_2 'free' region, where the SiO_2 had partially delaminated. Figure 6 (e) follows the same pore in the SiO_2 'capped' region, where the SiO_2 remained intact. A selection of the SEM images used for each reconstruction is presented in Figures 6 (a) to (c). From these volume reconstructions, the morphology of the selected pore may be followed along its entire length. This analysis revealed a straight horizontal pore in the stress relieved region, from which the SiO_2 cap had delaminated. The region extended for several microns, which was observed by this sectioning. As this reconstruction process was continued into the region where the SiO_2 cap had remained intact, a change in morphology as the pore splits in two can be observed in detail. The ability of the dual beam FIB sectioning/*in-situ* imaging method to reconstruct a region with extremely high site selectivity is apparent from this work. This capability makes this technique particularly powerful compared to other techniques used to image buried features, *e.g.* TEM cross sectional imaging.

To confirm that the volume reconstructions were accurate representations of the pore lengths, longitudinal TEM cross sections were taken to provide 2 D imaging along this length, as displayed in Figures 6 (f) to (h). Again, long, straight horizontal pores were observed in the

delaminated and presumably stress-relieved region. The estimated points of constraining contact with the upper and lower silicon oxide are indicated in the Figure 6 (h) with red arrows. For this experiment, the anodised region extends well under the SiO_2 capping film by ~1 μm. At its furthest extent on the left of the image where delamination has ceased, pore splitting has clearly begun.

From this cross-sectional analysis we propose a mechanism for the formation of pores under constrained and constrain-relieved conditions, as outlined schematically in Figure 7. During constrained pore growth of type I substrates, the forbidden flow of oxide along the Al/SiO_x interface induces oxide flow towards the pore centre, as indicated by white arrows in Figure 7 (b), and consequently dendritic pore morphology results. In the case of type II substrates, an anodisation front and a mechanical delamination front both travel horizontally along the Al finger length, as indicated by the blue and purple arrows, respectively, in Figures 7 (d) and (e). At the start of the anodisation process, these two fronts are very close together, the anodisation front just ahead of the delamination front (Figure 7(d)). The fact that ordered pores arise very quickly, within the first 3 μm of our system compared to tens of microns typical for vertical anodisation, suggests that the mechanically constraining silicon oxide layers play an important role in the establishment of an ordered array. It is currently accepted that the origin of this self-ordering is pore-to-pore repulsion arising from plastic flow of alumina at pore cell walls. In our experiments, the intimate presence of surrounding hard walls bounding the plastic flow of alumina establishes this repulsive ordering after a short duration of pore growth. However, this ordering influence also restricts the plastic flow of alumina behind the anodisation front, leading to bifurcation and eventually meandering in the pore growth, for pores constrained throughout their length (type I substrates). Only by stress release through delamination is this effect suppressed, as outlined by the flow of oxide along

the pore side walls, indicated by white arrows in Figure 7 (d), leading to the formation of long, straight, ordered pore formation. Our results clearly show that the loss of this delamination front quickly results in ‘fish-bone’ branching and meandering pore growth, as depicted in Figure 7(e).

4. Conclusions

In summary, we have studied the behaviour of planar pore formation in AAO in a mechanically constrained environment. Structural characterisation indicates that the mechanical constraint strongly affects the morphology and dynamics of pore formation. Mechanical coupling between the confining silicon dioxide and anodised aluminium layers imposes an overall stress on the anodisation and restricts the flow of oxide at the interfaces. Consequently, oxide flows towards the pore centre and a dendritic ‘fish-boned’ pore morphology results. However, the release of this constraint by an interfacial fracture tip that closely tracks the anodisation front can result in the fortuitous condition of long, straight pores that are nevertheless well ordered. Figure 7 schematically summarises the conditions which lead to both disordered pores with ‘fish-boned' pore morphology and long, straight ordered pores. These ordered planar pores have been characterised by electron microscopy and for the first time an array of ~3 μm long horizontal pores has been shown using 3 D reconstruction and by cross sectioning along the pore axes. This study contributes a deeper understanding of planar pore formation in AAO films in a mechanically constrained environment, which is important when considering the applications of AAO as a template/host material in various device architectures.

Acknowlegdements

We acknowledge financial support from the Irish Research Council for Science, Engineering and Technology (IRCSET) and CRANN/SFI (Project 08-CE-I1432). We also acknowledge the National Access Program (NAP) under which the substrates were provided by Tyndall National Institute (NAP 115). We thank Drs Richard Hobbs and Justin O'Byrne for TEM imaging. This research was also enabled by the Higher Education Authority Program for Research in Third Level Institutions (2007-2011) 35 via the INSPIRE program.

Figures

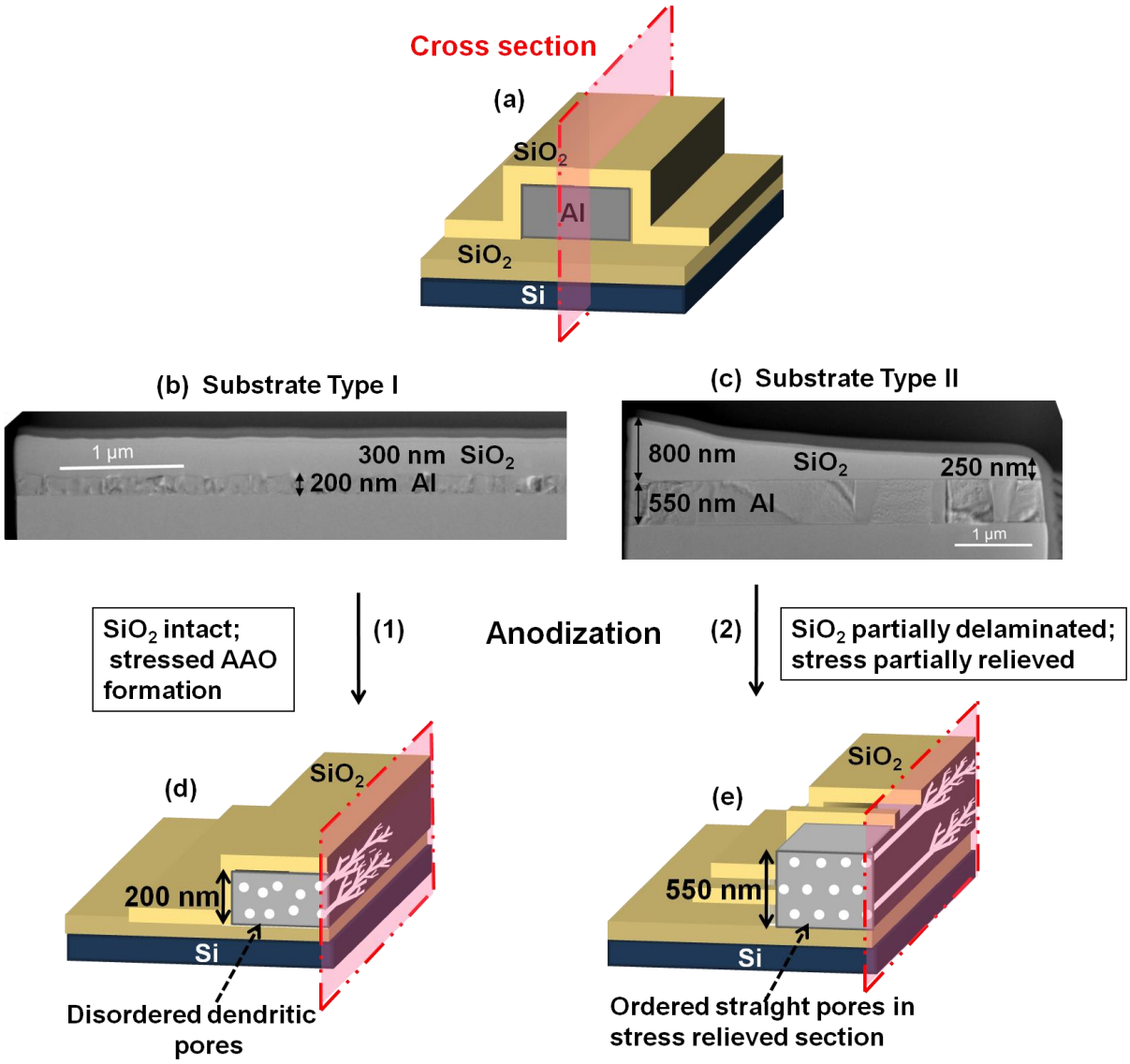

Figure 1. Schematic depiction of the samples before (a) and after (d) & (e) anodisation. Two substrate types were used for anodisation, detailed by cross sectional TEM analysis along the Al finger (b) and (c). Paths 1 and 2 outline the results obtained for the two substrate types.

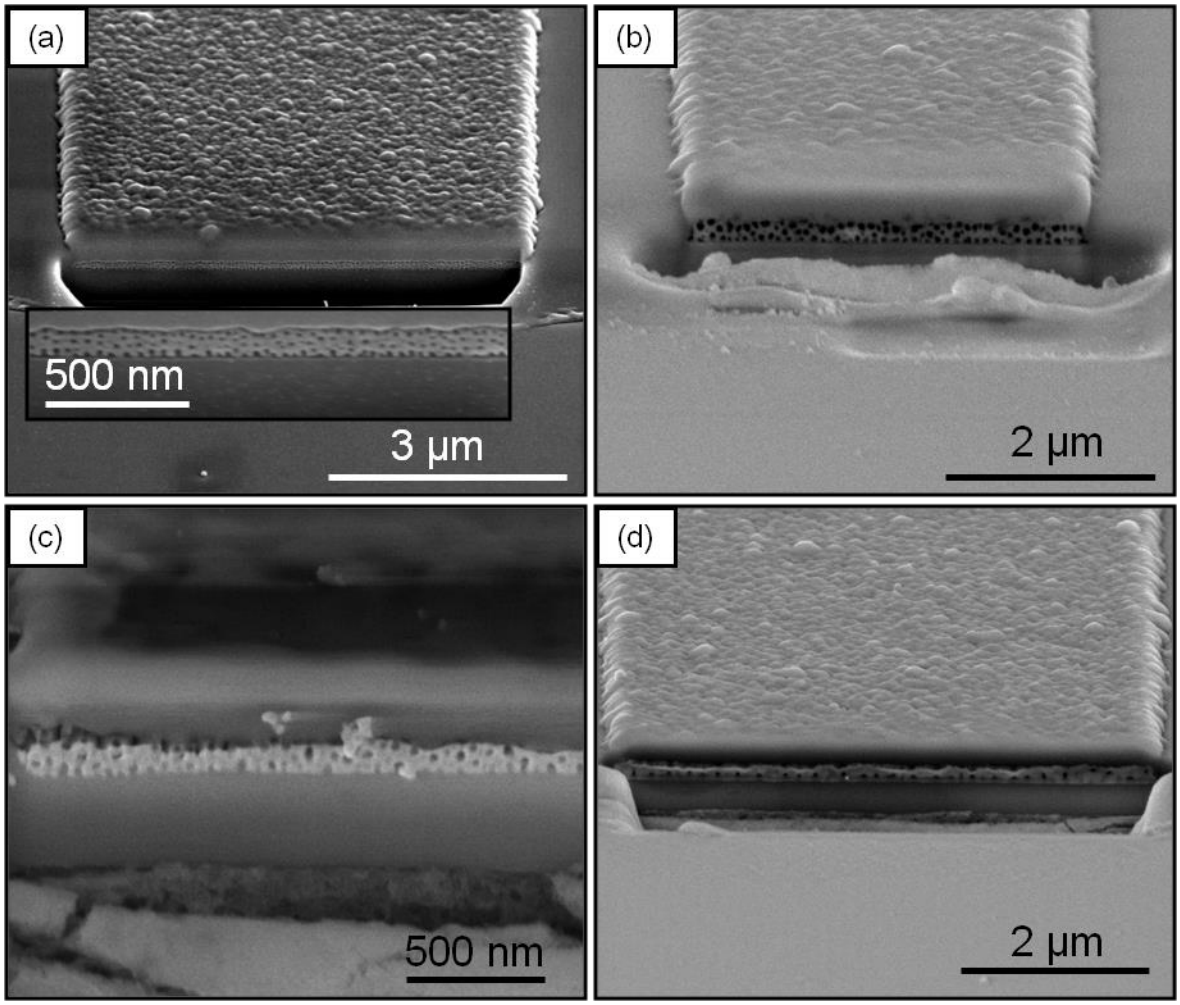

Figure 2. 'Front on' SEM images of 200 nm thick fingers (substrate type I) anodised at various conditions: (a) 20 V H_2SO_4 with higher magnification inset, (b) 40 V $H_2C_2O_4$, (c) 80 V H_2SO_4 and (d) 130 V $H_2C_2O_4$. Images were acquired at a tilt of ~45º to the electron beam.

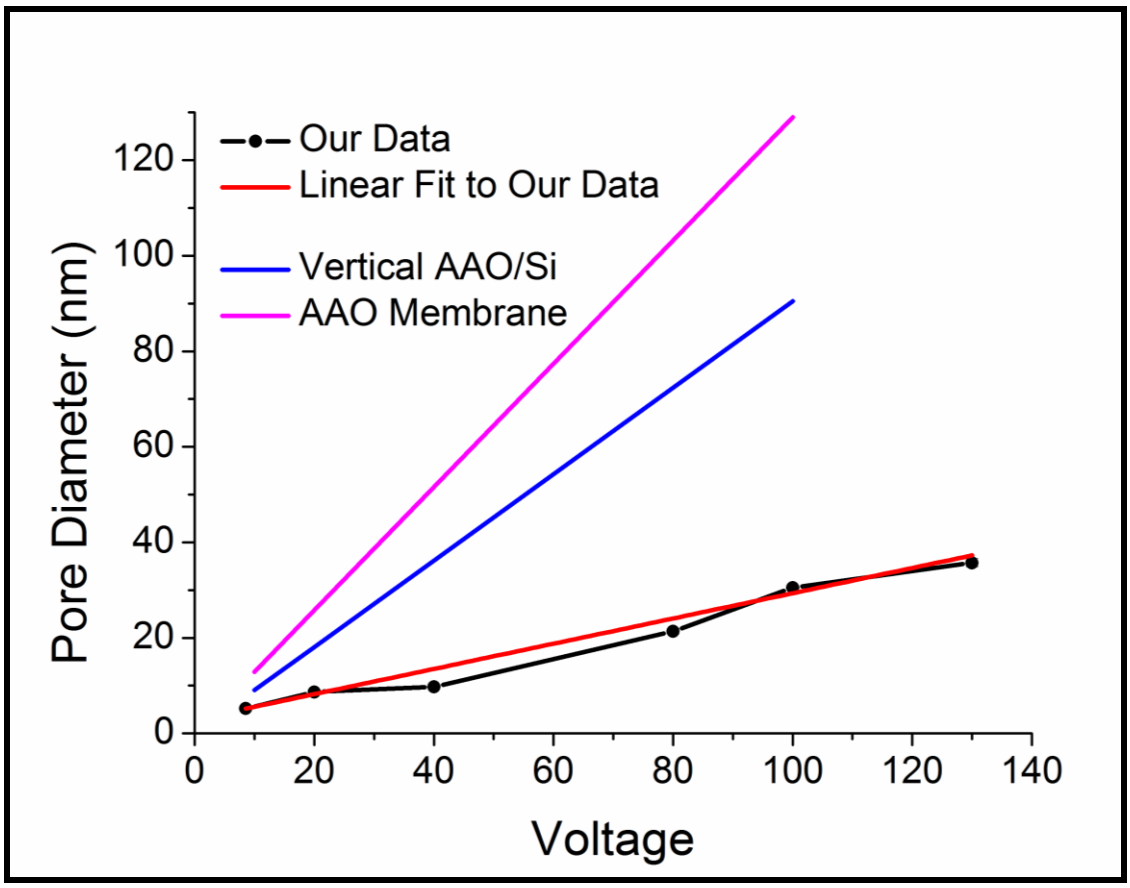

Figure 3. Graph of pore diameter vs. voltage for substrates containing 200 nm thick Al fingers anodised at constant potential ranging between 8.5 and 130 V (black trace), including linear fit (red trace) to the data and traces of this empirical law for free standing AAO membranes (magenta)[27] and for supported thin films (blue).[28] Electrolytes were employed based on the applied voltage ranges for self-ordering regimes.

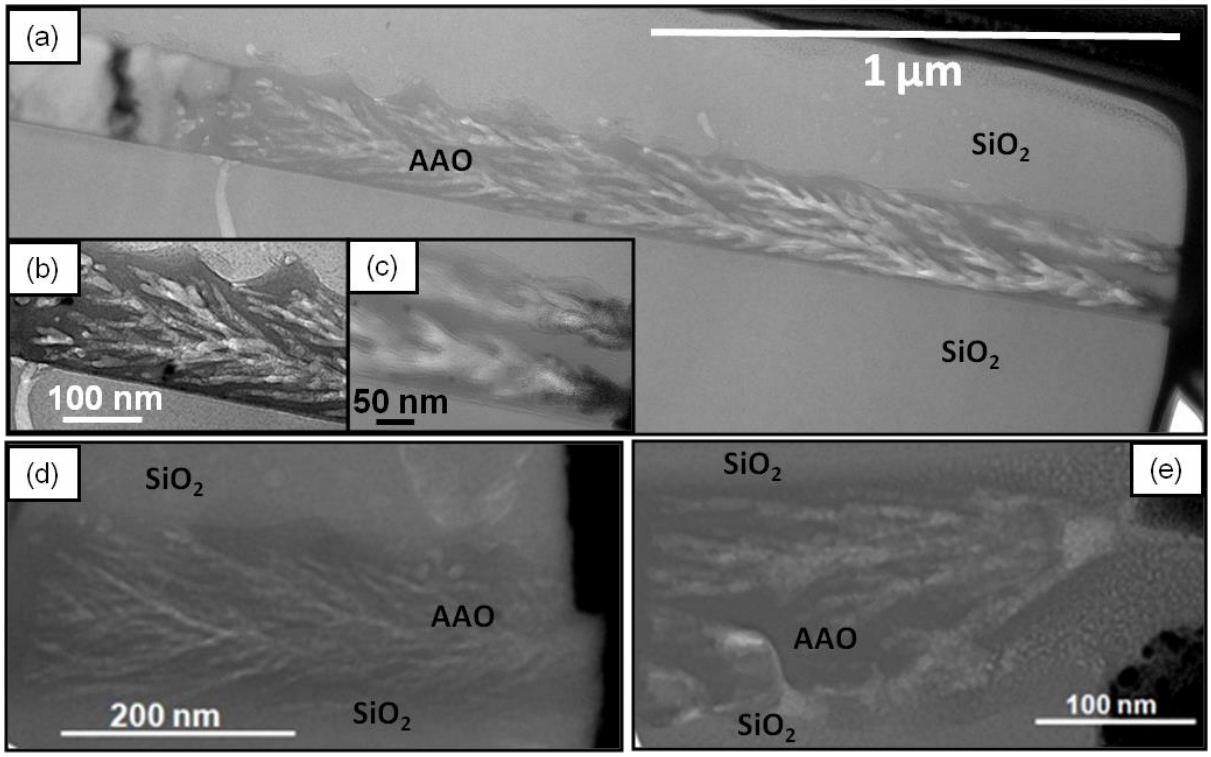

Figure 4. Longitudinal TEM cross sections of 200 nm thick films (substrate type I) for various anodisation conditions: (a) 40 V $H_2C_2O_4$ with (b) and (c) higher magnification inset of the branched ends and pore openings, (d) 10 V H_2SO_4, (e) 130 V $H_2C_2O_4$.

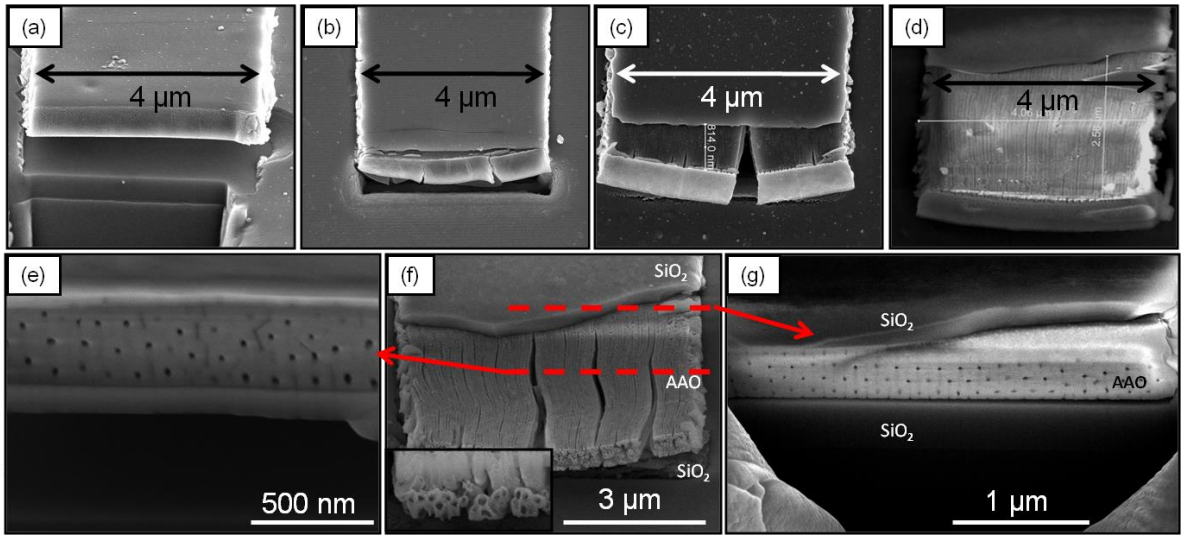

Figure 5. 'Front on' SEM images of 550 nm thick Al fingers (substrate type II) anodised at (a) 20 V, (b) 40 V, (c) 60 V and (d) 80V with H_2SO_4. (f) SEM of a different sample anodised at 80 V with higher magnification inset. (e) and (g) Transverse SEM cross sections exposed by FIB milling at the positions indicated with dashed red lines on (f).

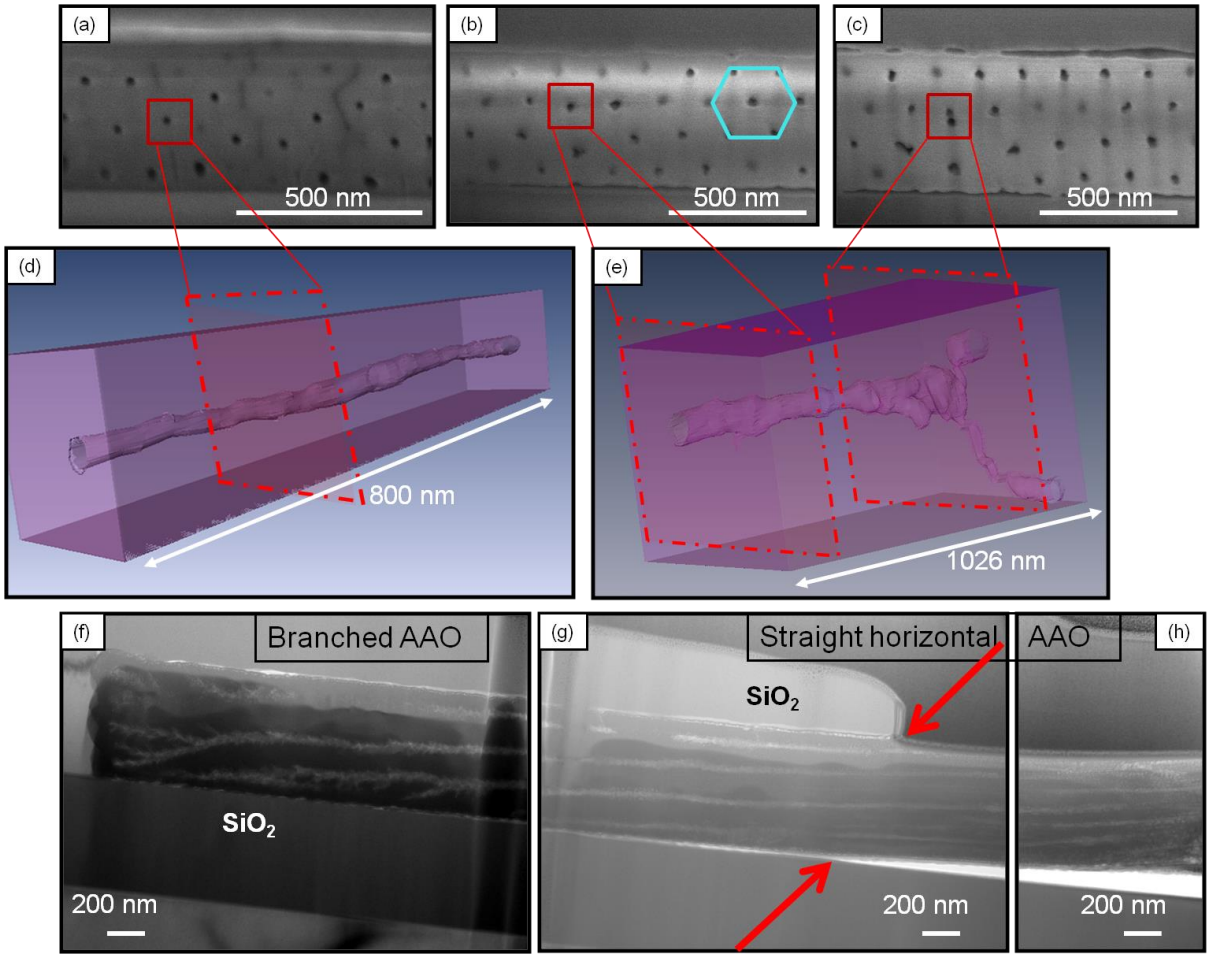

Figure 6. (a) to (c) SEM images exposed by FIB serial sectioning which were used to reconstruct volumes (d) and (e). The sectioned sample, substrate type II, was anodised at 80 V with 20 wt% H_2SO_4 for 7 h. (d) Reconstructed pore volume sectioned in the 'SiO_2 cap- free' region and (e) reconstructed pore volume sectioned in the SiO_2 covered region of the same sample. (f) to (h) Longitudinal TEM Cross Sections of another finger anodised under the same conditions. Red arrows indicate where delamination occurred.

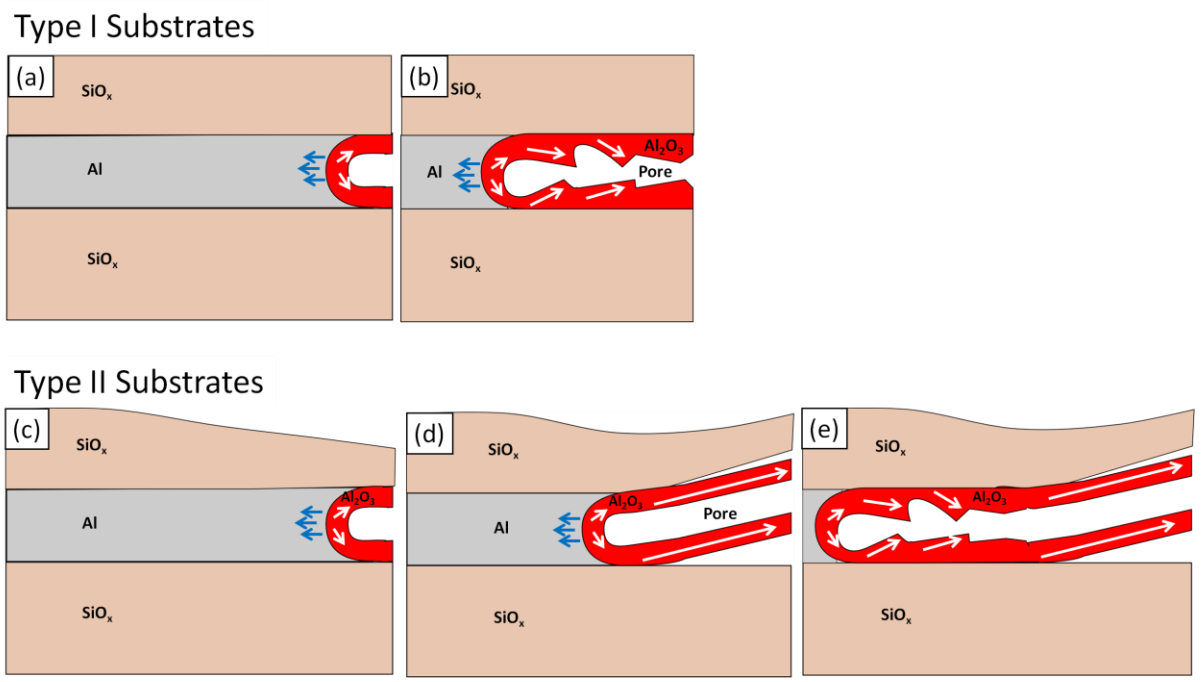

Figure 7. Mechanism of constrained (a) and constrain-released (b) pore growth. The white arrows indicate the direction of oxide flow during anodisation in each case.

References

[1] Davidson FMI, Schricker AD, Wiacek RJ and Korgel BA 2004 *Adv. Mater.* **16** 646

[2] Goodey AP, Eichfeld SM, Lew K-keong, Redwing JM and Mallouk TE 2007 *J. Am. Chem. Soc* **129** 12344

[3] Petkov N, Birjukovs P, Phelan R, Morris MA, Erts D and Holmes JD 2008 *Chem. Mater.* **20** 1902

[4] Shimizu T, Xie T, Nishikawa J, Shingubara S, Senz S and Gösele U 2007 *Adv. Mater.* **19** 917

[5] Barth S, Hernandez-ramirez F, Holmes JD and Romano-rodriguez A 2010 *Prog. Mater. Sci.* **55** 563

[6] Marquardt B, Eude L, Gowtham M, Cho G and Jeong HJ 2008 *Nanotechnology* **19** 405607

[7] Masuda H, Abe A, Nakao M, Yokoo A, Tamamura T and Nishio K 2003 *Adv. Mater.* **15** 161

[8] Rabin O, Herz PR, Lin Y-ming, Akinwande AI, Cronin SB and Dresselhaus MS 2003 *Adv. Func. Mater.* **13** 631

[9] Xu Q, Meng G, Wu X, Wei Q, Kong M, Zhu X and Chu Z 2009 *Chem. Mater.* **21** 2397

[10] Rodriguez AT, Chen M, Chen Z, Brinker CJ and Fan H 2006 *J. Am. Chem. Soc* **128** 9276

[11] Goring P, Pippel E, Hofmeister H, Wehrspohn RB, Steinhart M and Gosele U 2004 *Nano Lett.* **4** 1121

[12] Kim L, Kim J, Gu GH and Suh JS 2006 *Chem. Phys. Lett.* **427** 137

[13] Kline TR, Tian M, Wang J, Sen A, Chan MWH and Mallouk TE 2006 *Inorg. Chem.* **45** 7555

[14] Wade TL, Hoffer X and Mohammed AD 2007 *Nanotechnology* **18** 125201

[15] Masuda H, Nishio K and Baba N 1993 *Appl. Phys. Lett.* **63** 3155

[16] Xiang Y, Lee W, Nielsch K, Abstreiter G and Fontcuberta A 2008 *Phys. Stat. Sol. (RRL)* **2** 59

[17] Cojocaru CS, Padovani JM, Wade T, Mandoli C and Polytechnique E 2005 *Nano Lett.* **5** 675

[18] Gowtham M, Eude L, Cojocaru CS, Marquardt B, Jeong HJ, Legagneux P, Song KK and Pribat D 2008 *Nanotechnology* **19** 035303

[19] Xiang Y, Keilbach A, Codinachs LM, Nielsch K, Abstreiter G, Fontcuberta A and Bein T 2010 *Nano Lett.* **10** 1341

[20] Jessensky O, Muller F and Gosele U 1998 *Appl. Phys. Lett.* **72** 1173

[21] Garcia-vergara SJ, Clere DL, Hashimoto T, Habazaki H, Skeldon P and Thompson GE 2009 *Electrochim. Acta* **54** 6403

[22] Houser JE and Hebert KR 2009 *Nat. Mater.* **8** 415

[23] Sulka GD, Stroobants S, Moshchalkov VV and Borghs G 2004 *J. Electrochem. Soc.* **151** 260

[24] Park S-hyun, Lee Y, Lee J-kyu and Kim K-bum 2006 *Electrochem. Solid St.* **9** D31

[25] Barela MJ, Brevnov DA, Bauer TM, Lo GP and Atanassov PB 2005 *Electrochem. Solid St.* **8** C4-C5

[26] Oh J and Thompson CV 2011 *J. Electrochem. Soc.* **158** 71

[27] O'Sullivan J and Wood GC 1970 *P. R. Soc. Lon. Ser-A* **317** 511

[28] Robinson AP, Burnell G, Hu M and Macmanus-driscoll JL 2007 *Appl. Phys. Lett.* **91** 143123

[29] Fois G, Bolger CT, Holmes D and Cross GLW 2011 *J. Mater. Chem.* **21** 8772

[30] Oh J and Thompson CV 2011 *Electrochim. Acta* **56** 4044

[31] Zhu R, Zhang H, Chen Z, Kryukov S and Delong L 2008 *Electrochem. Solid St.* **11** K57

[32] Kim K, Kim M and Cho SM 2005 *Korean J. Chem. Eng.* **22** 789

[33] Lelonek M, Koppa O and Knoll M 2009 *Electrochim. Acta* **54** 2805

[34] Vrublevsky I, Parkoun V, Schreckenbach J and Marx G 2003 *Appl. Surf. Sci.* **220** 51

[35] Bradhurst DH and Leach JSL 1966 *J. Electrochem. Soc.* **113** 1245